

University of Windsor

Scholarship at UWindor

Electronic Theses and Dissertations

Theses, Dissertations, and Major Papers

1-1-1965

Electron spin resonance studies of ferric iron in cordierite.

Subhas Chandra Chakravartty
University of Windsor

Follow this and additional works at: <https://scholar.uwindsor.ca/etd>

Recommended Citation

Chakravartty, Subhas Chandra, "Electron spin resonance studies of ferric iron in cordierite." (1965).
Electronic Theses and Dissertations. 6377.
<https://scholar.uwindsor.ca/etd/6377>

This online database contains the full-text of PhD dissertations and Masters' theses of University of Windsor students from 1954 forward. These documents are made available for personal study and research purposes only, in accordance with the Canadian Copyright Act and the Creative Commons license—CC BY-NC-ND (Attribution, Non-Commercial, No Derivative Works). Under this license, works must always be attributed to the copyright holder (original author), cannot be used for any commercial purposes, and may not be altered. Any other use would require the permission of the copyright holder. Students may inquire about withdrawing their dissertation and/or thesis from this database. For additional inquiries, please contact the repository administrator via email (scholarship@uwindsor.ca) or by telephone at 519-253-3000ext. 3208.

ELECTRON SPIN RESONANCE STUDIES OF
FERRIC IRON IN CORDIERITE

BY

SUBHAS CHANDRA CHAKRAVARTTY

A Thesis
Submitted to the Faculty of Graduate Studies through the
Department of Physics in Partial Fulfillment
of the Requirements for the Degree of
Master of Science at the
University of Windsor

Windsor, Ontario

1965

UMI Number: EC52558

INFORMATION TO USERS

The quality of this reproduction is dependent upon the quality of the copy submitted. Broken or indistinct print, colored or poor quality illustrations and photographs, print bleed-through, substandard margins, and improper alignment can adversely affect reproduction.

In the unlikely event that the author did not send a complete manuscript and there are missing pages, these will be noted. Also, if unauthorized copyright material had to be removed, a note will indicate the deletion.

UMI[®]

UMI Microform EC52558

Copyright 2008 by ProQuest LLC.

All rights reserved. This microform edition is protected against unauthorized copying under Title 17, United States Code.

ProQuest LLC
789 E. Eisenhower Parkway
PO Box 1346
Ann Arbor, MI 48106-1346

Approved

F. Holuj
Dr. F. Holuj

S. N. Kalra
Dr. S. N. Kalra

N. E. Hedgecock
Dr. N. E. Hedgecock
(Supervisor)

120106

ABSTRACT

The electron paramagnetic resonance spectrum of Fe^{3+} impurity which enters substitutionally for the Al in a single crystal of cordierite $\text{Al}_3\text{Mg}_2(\text{Si}_5\text{Al})\text{O}_{18}$, has been examined at X-band frequency at room temperature. There are three sites of Al, two of them being crystallographically equivalent, the neighbourhood of which forms very distorted tetrahedra. Fe^{3+} spectra from these two equivalent sites are observed. Because of high crystal field splitting (large value of D) the usual Zeeman transitions are not observed, and only the low field doublets are present.

The spectrometer used is a simple bridge type spectrometer using a circulator in place of ordinary magic-T. The spectrum has been fitted to the spin-Hamiltonian $H = g\beta HS + D\left\{S_z^2 - \frac{1}{3}S(S+1)\right\} + E(S_z^2 - S_y^2)$. Energy level diagrams have been plotted for all the levels and along all the three magnetic axes. The observed and predicted positions of the transitions agree very closely in all cases. The parameter E/D and D have been obtained and are $E/D = 0.193 \pm .003$, $D = 15 \pm 5\text{Kg}$.

ACKNOWLEDGEMENT

The author wishes to express his sincere gratitude to Dr. N. E. Hedgecock for guidance and encouragement throughout the course of this work. Thanks are also due to Dr. H. Ogata for helping in computer programming.

TABLE OF CONTENTS

ABSTRACT	11
ACKNOWLEDGEMENT.....	iii
TABLE OF CONTENTS.....	iv
LIST OF FIGURES.....	vi
LIST OF TABLES.....	vii
CHAPTER	
I. INTRODUCTION.....	1
A. History of EPR.....	1
B. Paramagnetic Resonance.....	3
C. Resonance Condition.....	5
II. THEORY.....	8
A. Trivalent Iron.....	8
B. General Hamiltonian.....	8
C. Spin Hamiltonian.....	13
III. WORK IN STRONG CRYSTAL FIELDS.....	18
IV. CRYSTAL STRUCTURE.....	21
V. APPARATUS.....	26
A. Microwave Signal Components.....	28
B. Klystron.....	30
C. Detection System.....	33
D. Magnet.....	33
E. Cavity.....	34
VI. EXPERIMENTAL PROCEDURE.....	37
A. Operation of the Spectrometer.....	37
B. Alignment of the Crystal.....	39

C.	Measurement of the Magnetic	
	Field and Klystron Frequency.....	40
VII	RESULTS AND CALCULATIONS.....	43
A.	Results.....	43
B.	Calculations.....	48
C.	Errors.....	57
VIII	CONCLUSIONS.....	59
	BIBLIOGRAPHY.....	61
	VITA AUCTORIS.....	64

LIST OF FIGURES

4.1	STRUCTURE OF CORDIERITE AND BERYL.....	24
5.1	BLOCK DIAGRAM OF SPECTROMETER.....	27
5.2	PRINCIPLE OF AFC.....	31
5.3	CAVITY ASSEMBLY.....	35
7.1	SPECTRA OF CORDIERITE.....	44
7.2a	ANGULAR VARIATION OF g_{eff} VALUES ($H \perp b$).....	45
7.2b	ANGULAR VARIATION OF g_{eff} VALUES ($H \perp c$).....	46
7.3a	g_x FOR LOW FIELD DOUBLETS.....	49
7.3b	g_y FOR LOW FIELD DOUBLETS.....	50
7.3c	g_z FOR LOW FIELD DOUBLETS.....	51
7.4a	ENERGY LEVELS FOR $x \parallel H$	54
7.4b	ENERGY LEVELS FOR $y \parallel H$	55
7.4c	ENERGY LEVELS FOR $z \parallel H$	56

LIST OF TABLES

2.1	SPIN HAMILTONIAN MATRIX.....	15
2.2	TRANSFORMATION OF D AND E.....	16
4.1	ATOMIC POSITIONS IN CORDIERITE AND BERYL.....	22
7.1	EXPERIMENTAL RESULTS.....	48
7.2	DETERMINATION OF D AND η	53
7.3	COMPARISON OF EXPERIMENTAL & THEORETICAL RESULTS.	57

CHAPTER I

INTRODUCTION

A. History of EPR

Electron spin resonance or so called paramagnetic resonance was first discovered by Y.K. Zavoyskiy (1944). Zavoyskiy's discovery was preceded by some theoretical assumptions on the nature of the expected effect. Following the Stern-Gerlach experiments on the spatial quantization, Einstein and Ehrenfest advanced a number of arguments concerning quantum transitions between magnetic sublevels of atoms under the influence of equilibrium radiation. On the basis of these considerations, Dorfman suggested in 1923 the possibility of resonance absorption of electromagnetic waves by paramagnetic substances naming the phenomenon 'the paramagnetic effect'. The fundamental work by I. Waller in 1932, containing a quantum theory of paramagnetic relaxation in solids, served as a basis of the further development of the theory of dynamic phenomena in paramagnetic substances, in particular, of paramagnetic resonance.

Gorter(1936-1942), using frequencies of 10^6 - 3×10^7 c/s tried to observe the heat liberated by the paramagnetic substance. His experiments were unsuccessful because of

insufficient sensitivity and very low frequency.

In 1945, Zavoyskiy developed new and highly sensitive methods for the study of paramagnetic resonance. Instead of determining the amount of heat liberated, as did Gorter, he began to measure the weakening of the energy of the high frequency field as a result of absorption. In his first series of experiments, he used a 25-meter wavelength to observe absorption as a function of magnetic field in substances whose line widths were 50 gauss or larger, and a resonance line was scarcely discernible at such low frequencies, which correspond to a resonance peak of about 4 gauss. In the second series of his experiments, he found a maximum for Cu^{++} ion at 47.6 gauss, using a frequency of 133 Mc/s. Subsequently Zavoyskiy conducted experiments in the microwave region and observed clearly resolved resonance lines of 200 to 300 gauss in width in fields of about one kilogauss. In the U.S.A, Cummerow and Halliday (1946) observed clearly resolved resonance lines of Mn^{++} in $\text{MnSO}_4 \cdot 4\text{H}_2\text{O}$. They used a microwave resonance cavity excited at 2930 Mc/s. At the Clarendon laboratory, Bagguley and Griffiths (1947) observed the resonances of the paramagnetic Cr^{3+} ion in a chrome alum crystal at 3.18cm.wavelength. The experimental techniques and apparatus were perfected by the Oxford group, headed by Bleaney and Griffiths, while the work of Pryce, Stevens and others advanced the theoretical

understanding of the subject. Since then much work has been done in EPR, and the literature in the present day is extensive.

A number of review articles and books relating to EPR have been written, and these contain references to earlier work which give a full development of the subject. They are Bleaney and Stevens (1953), Bowers and Owen (1957), Orton (1959), Wertz (1955), Ingram (1955-1958), Bagguley and Owen (1957), Low (1960), Singer (1959), Pake (1962), Al'tshuler and Kozyrev (1964), Varian associates (1961).

B. Paramagnetic Resonance

Paramagnetic resonance is a very useful method for investigating many substances in the solid, liquid and gaseous states. In the solid state the experiments provide data on the forces between atoms of the solids. Paramagnetic resonance gives the most direct and accurate description of the ground state and of the effect of the crystalline environment on the energy levels of paramagnetic ion. The precision with which the paramagnetic resonance spectra can be measured enables one to determine the significant 'crystal-field' parameters in the theories of solid state interactions.

Electron spin resonance refers to the magnetic resonance of permanent magnetic dipole moments of electrons. If a paramagnetic substance having a total angular momentum \vec{J} is placed in a uniform magnetic field H_0 , then each of

its constituent paramagnets will have a ladder of $2J+1$ accessible levels. Using a high frequency oscillatory electromagnetic field, transitions can be induced among these $2J+1$ levels. This phenomenon of inducing transitions is termed as 'spin resonance'. This is termed as 'resonance' since absorption occurs only at the frequency corresponding to the energy level difference.

Paramagnetism occurs whenever a system has a resultant angular momentum. If this is of electronic origin, one speaks of electronic paramagnetism. Such paramagnetism is found:

1. In all atoms having an odd number of electrons; for example, in atomic nitrogen or hydrogen.
2. In ions having partly filled inner electron shells as in the transition groups.
3. In molecules having odd number of electrons, such as NO.
4. In a small number of molecules with an even number of electrons but having a resultant angular momentum, as in O_2 .
5. In free radicals, as in CH_3 . Such radicals are chemical compounds possessing unpaired electrons. They can often be produced in solutions or solids by nuclear radiation.
6. In color centers. These involve, in the main, electrons or holes trapped in various regions of the

lattice in a crystal.

7. In metals and semiconductors caused by conduction electrons.

C. Resonance Condition

For a free ion the total electronic angular momentum is given by $\vec{J} = \vec{L} + \vec{S}$, where \vec{L} and \vec{S} are the orbital and spin electronic angular momentum respectively. If such a free ion is placed in a magnetic field H , the energy levels are given by

$$W = g\beta HM, \quad 1.1$$

where g is the Lande' g factor given by

$$g = 1 + \frac{J(J+1) + S(S+1) - L(L+1)}{2J(J+1)} \quad 1.2$$

and $\beta = eh/4mc$ is the Bohr magneton, where e and m are the charge and mass of the electron, c is the velocity of light, h is Planck's constant, and M is the projection of the electronic angular momentum \vec{J} along the magnetic field direction. If an alternating field of frequency ν is applied at right angles to H , magnetic dipole transitions are induced according to the selection rule $\Delta M = \pm 1$. The fundamental equation for these transitions is $h\nu = W_1 - W_2$, where W_1 and W_2 are the energies of two consecutive energy levels. Hence, the condition for resonance in the isotropic case with no nuclear spin is

$$h\nu = g\beta H. \quad (1.3)$$

Energy is absorbed at resonance if the spin of the electron is flipped from a direction parallel to the magnetic field to that of antiparallel direction. When the converse occurs, one speaks of induced emission. The probabilities for emission and absorption are equal. However, for a system in thermal equilibrium, Boltzmann's statistics predict a greater population in the lower state, and consequently there is a greater absorption than emission of energy.

When the paramagnetic ion is placed in a crystal, the crystalline electric field removes most of the orbital degeneracy of the energy levels. Spin-orbit coupling also helps to remove some of the degeneracy. In many cases a single lower level degenerate with respect to spin only is left; all other levels are about 10^4 cm^{-1} higher. Hence, in these cases, only the ground state is populated at ordinary temperatures because of the Boltzmann distribution in population. Paramagnetic resonance takes place with ions in solids, the lowest level of which is usually degenerate with respect to spin only. The resonance condition for the solid state is again given by equation (1.3), but the g is now termed as the 'spectroscopic splitting factor' and is not given by expression (1.2) but is in general a tensor quantity. It effectively gives a measure of the rate at which the energy levels diverge with the applied magnetic

field. If the electron spins were absolutely free and had no coupling to any orbital motion then g value would be 2. A deviation from this value of 2 indicates some orbital effect is present. From the experimentally derived g values and their angular variations some information concerning the higher orbital state can be obtained.

CHAPTER II

THEORY

A. Trivalent Iron

In the present work the spectrum of Fe^{3+} , which substitutionally occupies the Al sites have been analyzed. Fe^{3+} is one of the common impurity ions which is found in many natural crystals. The spectrum is easily observable at room temperatures and has no hyperfine structure. In this group the 3d shell is in transition from $3d^1$ through $3d^9$, inclusive. The ion has five 3d electrons and a ground state ${}^6S_{5/2}$ indicating orbital angular momentum $L=0$ and spin $S=5/2$. Consequently the energy levels are six-fold degenerate and splits into six levels when the degeneracies are completely removed.

B. General Hamiltonian

The general theory of paramagnetic resonance in crystals is due to Abragam and Pryce (1951) and they express the different factors contributing to the total energy of an ion by the Hamiltonian as follows

$$\mathcal{H} = V_F + V_{LS} + V_{SS} + V_N + V_Q + V_H + V_{NH} \quad (2.1)$$

If, in addition, the ion is placed in a crystalline field, a term V_C due to the electrostatic interaction is added to

the Hamiltonian in (2.1). In expression (2.1) V_F represents the energy associated with the levels of the free ion and the splitting is usually of the order 10^5 cm^{-1} . V_{LS} represents the spin-orbit interaction which causes the energy to deviate from its spin-only value and is of the order of 10^2 cm^{-1} . V_{SS} is the spin-spin interaction of the electrons themselves and is usually very small. The term V_H given by $\beta H(\vec{L} + 2\vec{S})$ represents the Zeeman term and arises from the action of the external magnetic field on the electrons. The last term V_{NH} is the interaction of the external magnetic field H with the nucleus and is given by $-\gamma_N \beta_N H I$. Since Fe^{3+} has zero nuclear magnetic dipole moment, V_{NH} , as well as the dipole-dipole interaction V_N between the nuclear moment and magnetic moments of the electrons is zero. Also, since the nuclear electric quadrupole moment is zero, the interaction V_Q of the quadrupole moment Q of the nucleus with the electrostatic field gradient is zero. The resultant Hamiltonian is, therefore, given by

$$\mathcal{H} = V_F + V_{LS} + V_{SS} + V_H + V_C \quad (2.2)$$

The Coulomb term V_F is given by

$$V_F = \sum_{k=1}^N (p_k^2/2m - Ze^2/r_k) + \sum_{k,j=1}^N e^2/r_{kj} \quad (2.3)$$

Here, p_k is the linear momentum of the k th electron and r_k is the radius vector extending from the nucleus to the electron. The whole expression is summed over all N electrons;

k and j refer to the electron in the ion. This Coulomb repulsion is different for different states of the same configuration of the same electron and correspondingly leads to various energy levels and term values. The term V_{LS} is given by

$$V_{LS} = \sum_{jk} a_{jk} \mathbf{l}_j \cdot \mathbf{s}_k + b_{jk} \mathbf{l}_j \cdot \mathbf{l}_k + c_{jk} \mathbf{s}_j \cdot \mathbf{s}_k \quad (2.4)$$

where a_{jk} , b_{jk} and c_{jk} are constants, \mathbf{l} and \mathbf{s} represent the orbital and spin angular momentum and related to \mathbf{L} and \mathbf{S} by the relations $\vec{\mathbf{L}} = \sum_k^N \vec{\mathbf{l}}_k$ and $\vec{\mathbf{S}} = \sum_k^N \vec{\mathbf{s}}_k$.

If, however, one is restricted to states of definite $\vec{\mathbf{L}}$ and $\vec{\mathbf{S}}$ of the same configuration, the spin-orbit interaction can be written $\lambda \vec{\mathbf{L}} \cdot \vec{\mathbf{S}}$, where λ is a spin-orbit constant for a given ion. Pryce has also considered the very small spin-spin term written as

$$V_{SS} = \sum_{jk} \frac{\mathbf{s}_j \cdot \mathbf{s}_k}{r_{jk}^2} - \frac{3(\mathbf{r}_{jk} \cdot \mathbf{s}_j)(\mathbf{r}_{jk} \cdot \mathbf{s}_k)}{r_{jk}^5} \quad (2.5)$$

The crystalline field is regarded as arising from a system of point charges surrounding the paramagnetic ion. This sets up a static field which acts on the paramagnetic ion and changes the electronic orbit. Usually perturbation theory (Pryce, 1950) is used to calculate the effect of the crystalline field. It is essential, therefore, to know the relative orders of magnitude of the various terms in the Hamiltonian. Experimentally crystalline fields have been

found to fall into three groups. (a) Strong fields such that V_C is of the order of the energy of the mutual interaction between the electrons, that is 10^4 cm^{-1} . (b) Medium fields in which the Stark splittings are of the same order of magnitude (or slightly smaller) than the intervals between multiplets arising from the same electron configuration. Here perturbation theory is applied before calculating V_{LS} . (c) Weak fields in which the Stark splittings are small compared to the separation between the spin-orbit multiplets, i.e. $V_C \ll V_{LS}$. The notations strong, medium, or weak refer to the order of magnitude of the crystal field relative to the other terms in the Hamiltonian. The point at which the crystalline field will be used as a perturbation depends on the relative magnitude consideration.

If the point charges are regarded as not overlapping the paramagnetic ion, the electrostatic potential is then a solution of Laplace's equation $\nabla^2 V = 0$. The solutions can be expressed in terms of spherical harmonics in the form

$$V = \sum_n \sum_{m=-n}^n \sum_k A_n^m r^n Y_n^m(\theta_k, \phi_k) = \sum_n \sum_m V_n^m \quad (2.6)$$

where the summation k is over all the electrons, and the normalized harmonics are defined as

$$Y_n^m(\theta_k, \phi_k) = (-1)^n \left[\frac{1}{4\pi} \frac{(2n+1)(n-m)}{(n+m)} \right]^{1/2} P_n^m(\cos\theta) e^{im\phi} \quad (2.7)$$

where ϕ, θ represent the usual angles in the spherical polar coordinates and the suffix k refers to the k th electron.

However, it is not necessary to consider all the terms, since symmetry properties reduce the number of terms considerably. For the d and f electrons only expansions upto $n = 4$ and $n = 6$ respectively need to be considered. This is because of the fact that the wave functions of the electrons can also be expanded in harmonic functions,

$$\Psi_l^i \sim R(r_i) Y_l^i(\theta_i, \phi_i); \quad (2.8)$$

where $R(r_1)$ refers to the radial part of the wave function. The matrix elements are of the form $\Psi_l^i V_n \Psi_l^i$ and are, therefore, zero for all potentials for which $n > 2l$. Also all terms with odd n must vanish, since the product is unchanged by inversion, whereas the odd rank terms of the potential change sign. Even if there is no center of symmetry, the odd terms are still zero but there now may be terms from the admixture of higher levels. The term $n = 0$ only adds a constant to the expansion and adds nothing of significance. For the iron group, i.e. for d electrons, only values of 2 and 4 need to be considered, and hence

$$V_c = \sum_{m=0}^m \sum_{\pm 2}^k A_2^m r^2 Y_2^m + \sum_{m=0}^m \sum_{\pm 2, \pm 4}^k A_4^m r^4 Y_4^m \quad (2.9)$$

Moreover, the symmetry of V_c must be the same as that of the crystalline field, and in many cases this further restricts the number of terms in V_c . In particular, for

the present case of rhombic symmetry, only the terms with $m = 0, \pm 2$ and ± 4 need to be considered. For the sake of simplicity the terms with $l = 4$ have not been considered in the present case. Their contribution is presumably much smaller than the $l = 2$ terms, and as will be seen later, can not be determined from the experimentally available results.

C. Spin Hamiltonian

The general Hamiltonian expressed in eqn.(2.1) is in general very complicated. Pryce (1950) and Abragam and Pryce have developed a very useful method for carrying out perturbation calculation, and have applied this specially to iron group. The spin Hamiltonian thus obtained is, in fact, a short hand description of the experimental results. In the actual experiment the parameters in the spin Hamiltonian, that is g factor, the initial splittings, the hyperfine structure constants are obtained. The task is then to find a model of a crystal field which corresponds to the spin Hamiltonian and which explains the observed parameters.

Abragam and Pryce first transforms the various terms in the Hamiltonian (2.1) into expressions involving the appropriate angular momentum operators \vec{L} , \vec{S} , \vec{J} without giving them a definite representation and then use perturbation theory. In the resulting spin Hamiltonian, the

splitting of the effective spin levels by H is represented by energy operators

$$\mathcal{H} = \beta (g_z^H S_z + g_z^H S_z + g_z^H Y_z) \quad (2.10)$$

The spin Hamiltonian also contains terms which must conform to the local symmetry about the ion in the crystal. In Cordierite there is an axial symmetry with a large rhombic term. Considering all these terms, the spin Hamiltonian, for this case, can be written as

$$\begin{aligned} \mathcal{H} = \beta (g_x^H S_x + g_y^H S_y + g_z^H S_z) + D \left[S_z^2 - \frac{1}{3} S(S+1) \right] \\ + E (S_x^2 - S_y^2) \end{aligned} \quad (2.11)$$

where the D term is the contribution that would arise from a crystalline field of purely axial symmetry, and the E term is that due to a rhombic component of the crystalline field. The suffixes x, y, z refer to the three magnetic axes associated with the site of the ion in the crystal.

If the direction of the magnetic field is along the z magnetic axis of the crystal field, then eqn.(2.6) reduces to

$$\mathcal{H} = g_z \beta H S_z + D \left[S_z^2 - \frac{1}{3} S(S+1) \right] + E (S_x^2 - S_y^2) \quad (2.12)$$

This Hamiltonian must be expressed in matrix form and then diagonalized to find the energy levels. To obtain the matrix form of (2.12) we note that

$$\langle \pm M | S_z | \pm M \rangle = \pm M \quad (2.13)$$

and also the diagonal elements of the operator $\{S_z^2 - \frac{1}{3}S(S+1)\}$ are given, for $S = \frac{5}{2}$, by

$$\begin{aligned} \left\langle \pm \frac{1}{2} \left| S_z^2 - \frac{1}{3} S(S+1) \right| \pm \frac{1}{2} \right\rangle &= -\frac{8}{3} \\ \left\langle \pm \frac{3}{2} \left| S_z^2 - \frac{1}{3} S(S+1) \right| \pm \frac{3}{2} \right\rangle &= -\frac{2}{3} \\ \left\langle \pm \frac{5}{2} \left| S_z^2 - \frac{1}{3} S(S+1) \right| \pm \frac{5}{2} \right\rangle &= \frac{10}{3} \end{aligned} \quad (2.14)$$

The off-diagonal elements of the operator $(S_x^2 - S_y^2) = \frac{1}{2}(S_+^2 - S_-^2)$, where $S_{\pm} = (S_x \pm iS_y)$, are given by

$$\begin{aligned} \left\langle \pm \frac{3}{2} \left| \frac{1}{2} (S_+^2 - S_-^2) \right| \mp \frac{1}{2} \right\rangle &= 3\sqrt{2} \\ \left\langle \pm \frac{5}{2} \left| \frac{1}{2} (S_+^2 - S_-^2) \right| \mp \frac{1}{2} \right\rangle &= \sqrt{10} \end{aligned} \quad (2.15)$$

Using these results and rearranging, the final form of the matrix is shown in table (2.1)

Table 2.1

$ \pm 5/2\rangle$	$ \pm 1/2\rangle$	$ \mp 3/2\rangle$
$ \pm 5/2\rangle \pm \frac{5}{2}g_z\beta H_z + \frac{10}{3}D$	$\sqrt{10}E$	0
$ \pm 1/2\rangle \quad \sqrt{10}E$	$\pm \frac{1}{2}g_z\beta H_z - \frac{8}{3}D$	$3\sqrt{2}E$
$ \mp 3/2\rangle \quad 0$	$3\sqrt{2}E$	$\mp \frac{3}{2}g_z\beta H_z - \frac{2}{3}D$

The advantage of writing the matrix in the above form lies in the fact that diagonalization of the Hamiltonian requires the solution of two cubic equations, rather than the formidable task of solving one sixth order equation.

If the direction of the magnetic field is along the x or y magnetic axis, the Hamiltonian matrix (table 2.1) must be modified by replacing g_z by g_x or g_y and transforming D and E according to the following table (Bleaney and Bowers, 1952).

Table 2.2

	X-direction	Y-direction
D	$-\frac{1}{2} (D - 3E)$	$-\frac{1}{2} (D + 3E)$
E	$\frac{1}{2} (D + E)$	$\frac{1}{2} (D - E)$

The designation of the magnetic axes is somewhat arbitrary and is made as follows: since $S(S + 1) = S_x^2 + S_y^2 + S_z^2$, the spin Hamiltonian in zero magnetic field can be written in the form

$$A S_x^2 + B S_y^2 + C S_z^2 \quad (2.16)$$

It is always possible (Wickman, et.al; 1965) to choose a coordinate system such that $|C| \gg |B| \gg |A|$.

Furthermore , with this choice $E \leq \frac{1}{3}D$. This amounts to defining the Z-axis as that about which the symmetry is closest to axial.

CHAPTER III

WORK IN STRONG CRYSTAL FIELDS

The present work is one in a series of investigations of transition elements in natural silicates. Silicates, being complicated in structure, have not yet been thoroughly investigated. The particular silicate, cordierite, belongs to the iolite class and has been found to have Fe^{3+} and Mn^{2+} as paramagnetic impurities. The spectrum of Mn^{2+} is of the usual type, containing five groups of six lines. In the case of Fe^{3+} only two pairs of lines have been observed at very low fields instead of the usual five lines for each site of an iron ion. This immediately suggests that the Fe^{3+} ions are experiencing a very high crystal field. In the present work only the spectrum due to Fe^{3+} has been analyzed.

To date only a few cases of high crystal field effects on paramagnetic ions have been reported. In general, as is expected, the lines are observed at comparatively low fields. Such high crystal field effects were first reported by Sands (1955) in his investigation of silica glasses by EPR. He reported two resonance lines, one at $g = 4.2$ and the other at $g = 6$. Bennet and others (1957), in their investigation of hemoglobin and its derivatives by the EPR method, found lines with effective g

values which were interpreted by Griffith (1956) as consistent with a large crystal field splitting of the $S = \frac{5}{2}$ sextet in Fe^{3+} . Castner et al (1960) reexamined resonance in silica-glass samples containing known amounts of Fe^{3+} and found that this ion is responsible for an intense resonance at $g = 4.27$. More recent work in large crystalline fields includes the work on amethyst by Barry et al (1965), on ferrichrome 'A' by Wickman et al (1965) and on andalusite by Holuj (1965). In the first two cases the results were interpreted as arising from a large E term in the spin Hamiltonian. In these cases the magnetic axes were not defined in the manner described on page 17, which accounts for $E/D > \frac{1}{3}$ as observed by these workers.

Wickman et al, in their work with ferrichrome 'A', investigated the spectrum of Fe^{3+} in a strong crystalline field. A prominent line of 400 gauss width located at $g = 4.3$ was observed at all temperatures, while at 1°K additional resonances at g values of 9.6, 1.3, 1.0 was observed. The spectra were interpreted by assuming a spin Hamiltonian containing crystal field terms large compared with the Zeeman splittings; the crystal field situation is intermediate between the axial symmetry with

$$\mathcal{H} = D \left\{ S_z^2 - \frac{1}{3}S(S+1) \right\} + g\beta SH$$

and the model proposed by Castner, Newell and others to explain iron resonances occurring at $g = 4.3$, with $E(S_x^2 - S_y^2) + g\beta SH$. They computed g values, energy eigenvalues and eigenfunctions to be expected for the region between these two extremes, and

the results are useful in interpreting similar spectra due to iron situated in strong crystal fields of low symmetry.

In his work with andalusite, Holuj observed eight resolved lines at most orientations of the crystal. He has reported the analysis of the most intense pair of lines which has been fitted to the Hamiltonian $\mathcal{H}(s) = \beta g_{\parallel} H_z S_z + \beta g_{\perp} (H_x S_x + H_y S_y) + D(S_z^2 - \frac{35}{12}) + E(S_x^2 - S_y^2)$. Based on the same arguments of Griffith he has pointed out that D must be very large.

In addition to this work with Fe^{3+} the only work so far reported is on Cr^{3+} in emerald by Geusic et al (1958). They obtained a very large value of $D = -26 \pm 1.0$ Kmo. The large zero field splitting observed for the Cr^{3+} ion in this crystal might suggest emerald as a possible material for use in the design of solid-state masers for high microwave frequency applications.

CHAPTER IV

CRYSTAL STRUCTURE OF CORDIERITE

Cordierite, a silicate belonging to the space group C_{2h}^{20} (D_{2h}^{20}) has the orthorhombic structure. This is a silicate of Al and Mg and contains a few molecules of water. Cordierite can be synthesized without crystal water by mixing pure oxides and heating the mixture at about 1600°C . The unit cell dimensions are given by Bystrom (1941) are

$$a = 17.06\text{\AA}, b = 9.69\text{\AA}, c = 9.37\text{\AA}$$

From the crystallographic considerations cordierite has been attributed a chemical formula $\text{Al}_3 \text{Mg}_2 (\text{Si}_5 \text{Al}) \text{O}_{18}$ having 4 molecules in the unit cell (Bragg - 1937). The structure of cordierite resembles very closely that of hexagonal beryl having chemical formula $2 (\text{Be}_3 \text{Al}_2 \text{Si}_6 \text{O}_{18})$. The 3 Be in beryl correspond to 3 Al in cordierite, and 2 Al to 2 Mg.

The atomic coordinates of cordierite are given in table 4.1 and are compared with those of beryl.

There appears to be an error in the coordinates given for the group O_v . In particular the value $X_{10} = -0.681$ is suspect. Using these coordinates, O_v come much closer to the other oxygens than ionic radii would allow, and do not correspond to their positions as

Table 4.1

Beryl	Cordierite
	Atomic positions $(0,0,0; \frac{1}{2}, \frac{1}{2}, 0) +$
4 Al in 4(c)	8 Mg in 8(g): $\pm(x_1, 0, \frac{1}{4}; \bar{x}_1, 0, \frac{1}{4})$
6 Be in 6(f)	4 Al _I in 4(b): $\pm(0, \frac{1}{2}, \frac{1}{4})$
	8 Al _{II} in 8(k): $\pm(\frac{1}{4}, \frac{1}{4}, z_2; \frac{1}{4}, \frac{3}{4}, \frac{1}{2} + z)$
12 Si in 12(l)	20 Si+4 Al in 8(l): $\pm(x_3, y_3, 0; x_3, \bar{y}_3, \frac{1}{2})$
	in 8(l): $\pm(x_4, y_4, 0; x_4, \bar{y}_4, \frac{1}{2})$
	in 8(l): $\pm(x_5, y_5, 0; x_5, \bar{y}_5, \frac{1}{2})$
12 O in 12(l)	8 O _I in 8(l): $\pm(x_6, y_6, 0; x_6, \bar{y}_6, \frac{1}{2})$
	8 O _{II} in 8(l): $\pm(x_7, y_7, 0; x_7, \bar{y}_7, \frac{1}{2})$
	8 O _{III} in 8(l): $\pm(x_8, y_8, 0; x_8, \bar{y}_8, \frac{1}{2})$
24 O in 24(m)	16 O _{IV} in 16(m): $\pm(x_9, y_9, z_9; x_9, y_9, \bar{z}_9;$ $x_9, \bar{y}_9, \frac{1}{2} + z_9;$ $x_9, \bar{y}_9, \frac{1}{2} - z_9)$
	16 O _V in 16(m): $\pm(x_{10}, y_{10}, z_{10}; x_{10}, y_{10}, \bar{z}_{10}$ $x_{10}, \bar{y}_{10}, \frac{1}{2} \pm z_{10})$
	$\pm(x_{11}, y_{11}, z_{11}; x_{11}, y_{11}, \bar{z}_{11};$ $x_{11}, \bar{y}_{11}, \frac{1}{2} \pm z_{11})$

with

$$x_1 = 0.333$$

$$z_2 = 0.250$$

$$x_3 = 0.190$$

$$y_3 = 0.063$$

$$x_4 = 0.126$$

$$y_4 = -0.255$$

$$x_5 = 0.062$$

$$y_5 = 0.316$$

$$x_6 = 0.032$$

$$y_6 = -0.284$$

$$x_7 = 0.126$$

$$y_7 = 0.189$$

$$x_8 = 0.158$$

$$y_8 = -0.095$$

$$x_9 = 0.240$$

$$y_9 = -0.090 \quad z_9 = 0.350$$

$$x_{10} = -0.681$$

$$y_{10} = -0.405 \quad z_{10} = 0.350$$

$$x_{11} = -0.167$$

$$y_{11} = -0.315 \quad z_{11} = 0.350$$

Also the interatomic distances in cordierite are given by

$$Si - O^{16}$$

$$1.65 - 1.67^{\circ}A$$

$$Si - O^8$$

$$1.63 - 1.64^{\circ}A$$

$$Al^4 - O^{16}$$

$$1.75A^{\circ}$$

$$Al^8 - O^{16}$$

$$1.81A^{\circ}$$

$$Mg - O^{16}$$

$$2.01, 2.03 \text{ and } 2.12A^{\circ}$$

$$\text{Shortest } O - O$$

$$\text{Distance: } 2.50A^{\circ}$$

indicated in Fig. 4.1(a). The oxygen atoms in this group are nearest neighbours for aluminum atoms in the (b) positions and for the magnesium atoms, neither of which are directly concerned in the present work.

Fig. 4.1(a) shows the projection of the crystal on the (001) plane for cordierite and is compared with

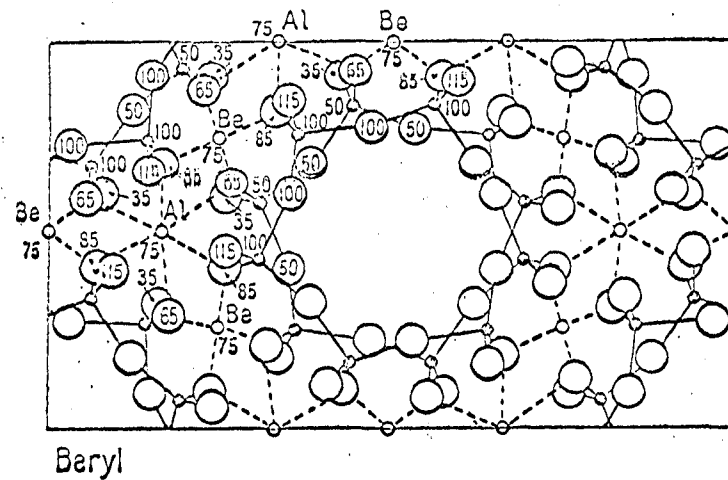
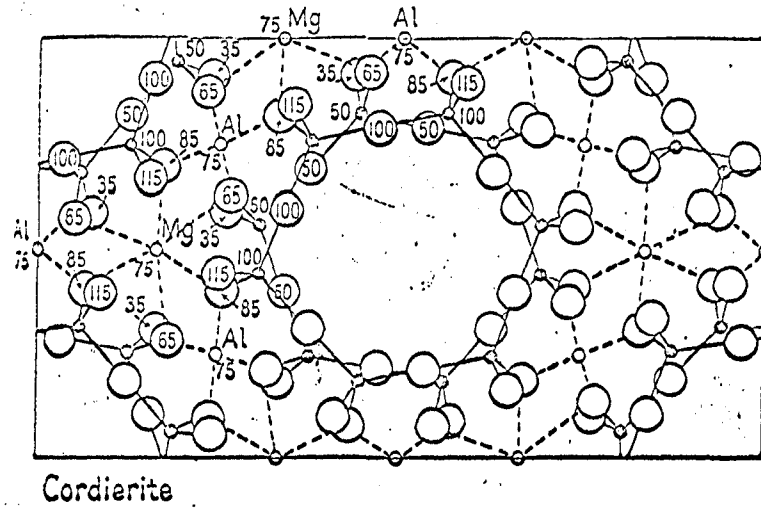


Fig. 4.1 The structure of cordierite and beryl. Projection on (001). The large circles are oxygen and the small black circles are silicon atoms. The figures denote the levels of the atoms in percent of c .

the structure of beryl in 4.1(b). The reflection planes are at heights 0, 50, 100. The striking similarity of both the structures are obvious and the symmetry of Be in beryl is the same as that of Al in cordierite and the symmetry of Al in beryl is the same as that of Mg in cordierite. In cordierite SiO_4 tetrahedra share oxygens to form Si_5O_{18} rings which have symmetry planes parallel to the base of the unit cell.

The symmetry at the Mg site includes a 3-fold axis parallel to the c-axis of the crystal. In cordierite the aluminium atoms occupying the b and k position appear to be all crystallographically equivalent related by 120° rotations about the c-axis. As discussed later, however, the experimental results indicate that the b and k positions are significantly different.

120106

UNIVERSITY OF WINDSOR LIBRARY

CHAPTER V

APPARATUS

The electron spin resonance spectrometer used is a simple bridge type as described by Feher (1957). The spectrometer operates at 3 cm wavelength corresponding to about 9000 mc/s frequency. The simple bridge type spectrometer has been used instead of the superheterodyne because the microwave power used was much lower than the saturation level of the sample. In such cases the bridge type spectrometer has sensitivity comparable with that of the superheterodyne (Feher - 1957) spectrometer; and at the same time is much easier to operate. A block diagram of the spectrometer is shown in Fig. 5.1(a).

In order to explain the function of the component parts of the spectrometer, it is convenient to consider the entire system to be divided into the following subdivisions. (A) The signal microwave components. (B) Klystron. (C) The detection system. (D) The magnet. (E) The cavity and goniometer.

A. Signal Microwave Component:

In the first phase of the experiment, the usual magic tee (Fig. 5.1(b)) was used in the bridge circuit in place of the circulator shown in Fig. 5.1(a). Power from the signal klystron, whose direction is indicated by the arrow of the ferrite isolator, enters the E arm of the magic tee. Half of the microwave power is transmitted down each side arm of the magic tee. There is connected to one side arm a slide-screw-tuner and a resonant cavity, and to the other side arm there is attached a crystal diode and a line termination. These elements, the attenuator, the slide-screw-tuner, the characteristic impedance of the line and the cavity can be considered as components of a radio-frequency bridge which can be so adjusted that no power appears in the H arm. At resonance, the bridge becomes unbalanced due to the absorption by the sample. Consequently microwave power appears in the H-arm. In the final phase of the work the magic tee was replaced by a circulator. A circulator is a comparatively recent device which, like the isolator, employs ferrite material and Faraday rotation to restrict the direction of flow of microwave power.

The circulator used was a Ferranti waveguide junction circulator, type 211XCD having 3 ports. The circulator works in the frequency range 8.2 - 100 Gc/sec with a minimum isolation of 20 db. Power entering port 1 can only emerge from port 2, power entering port 2 can

only emerge from port 3.

In the absence of saturation in the specimen, the theoretical sensitivity of the circuit (if the circulator is assumed to be perfect) is 6 db better than that of the best magic tee circuit, since in the magic-T circuit only half of the klystron power reaches the cavity and only half of the signal power reaches the detector. In our case the sensitivity was found to be about 4 times than that obtained by using the magic-T.

In addition to the components described, the EPR spectrometer has a few other accessories and measuring devices. There is a wavemeter next to the signal klystron for measuring the resonant frequency of the cavity and estimating roughly the Q. of the cavity. The straight arm H (Fig. 5.1 a) has a directional coupler, which is terminated by a matching stub and contains an IN 23 diode. Power from this diode is used for frequency stabilization of the klystron. The straight arm H is also similarly terminated and contains another IN 23 diode which detects the resonance signal. Provision is also made for a large 60 c/s modulation voltage to modulate the klystron reflector. When the klystron is modulated by this large voltage, the cavity mode can be displayed on the oscilloscope from the output of either of the detectors.

B. Klystron:

The microwave power source is a Varian 203/675 reflex klystron rated at power level of 50 milliwatts. The klystron is water-cooled and tunable over the range from 8500 mc/s to 9600 mc/s. The beam current used is approximately 30 milliamperes and is supplied by a Lambda regulated power supply, model 25. A six volt storage battery supplied the 0.4 - 0.5 amperes heater currents. The reflector voltage is provided by a shielded battery bank of various size dry cells. The reflector voltage can be increased or decreased in steps of 22.5 volts, or 3 volts, from a fixed voltage of -337.5 volts or -37.5 volts with respect to the ground or to the cathode, respectively. Also on the battery bank there is supplied a voltage that can be varied continuously over a 4.5 voltage range for fine tuning.

The frequency control system. An automatic frequency control system is included in order to provide optimum stability of the microwave oscillator. The klystron is locked onto the cavity resonant frequency. This eliminates the dispersion component of the EPR signals, removes frequency modulation noise and reduces microphonics. Such a system can be used to lock the frequency of the oscillator to that of the sample cavity with an accuracy of one part per million.

The block diagram of the automatic frequency control part is included in Fig. 5.1. A control frequency

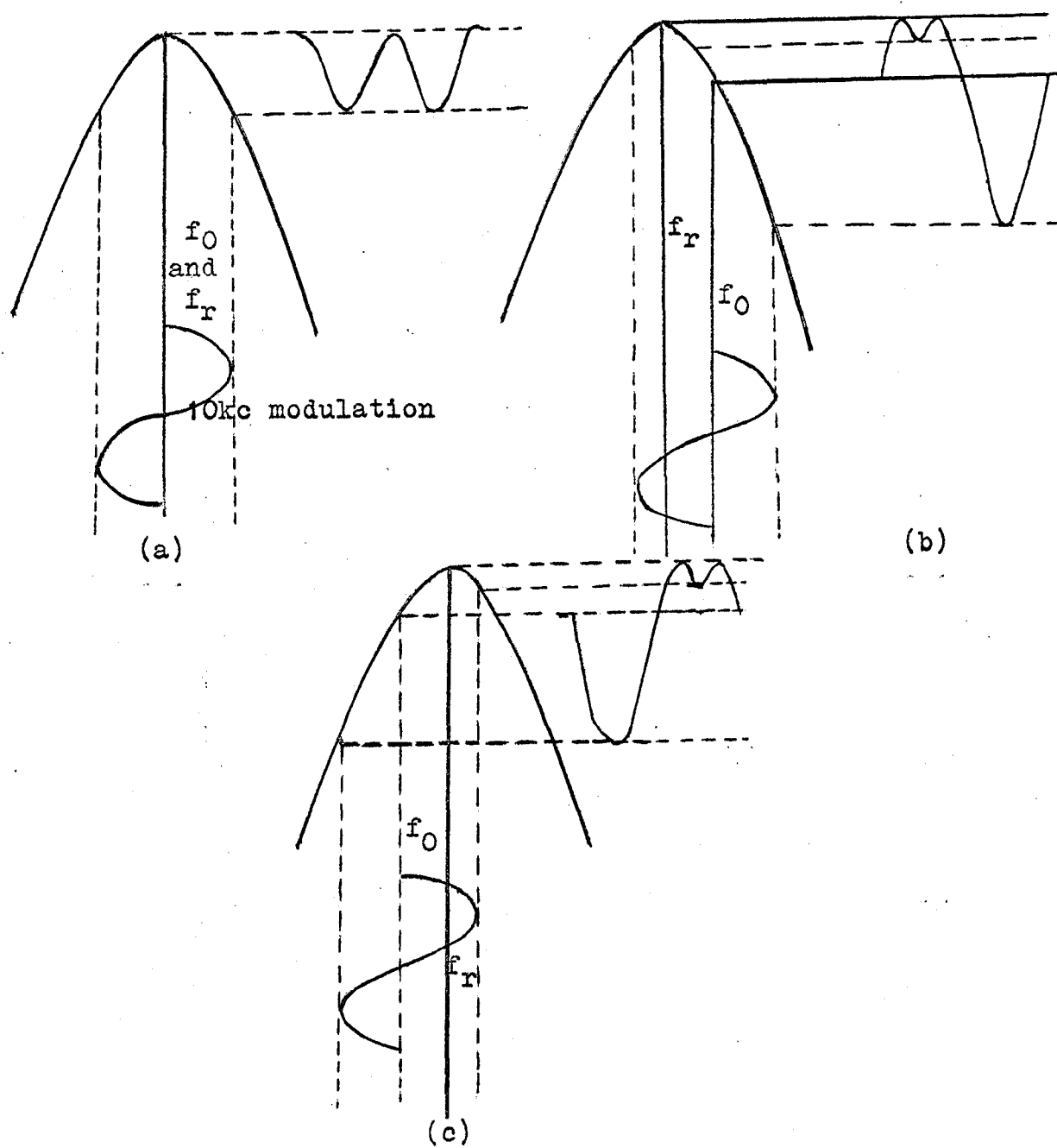


Fig 5.2 Principle of AFC.

of 10 kc/sec is provided by an oscillator (22) to both the AFC phase detector and power supply for the klystron reflector. In the AFC phase detector the 10 kc/sec voltage is used as a phase reference, while in the klystron power supply it is used to slightly modulate the reflector voltage, thus resulting in a small 10 kc/sec modulation of the klystron output frequency.

This frequency modulation causes the klystron frequency to vary with respect to the resonant frequency of the sample cavity. When the klystron center of frequency (f_0) corresponds to the resonant frequency of the sample cavity (f_r), the reflected power from the cavity is amplitude modulated at a frequency which is the second harmonic of 10 kc/sec (i.e. 20 kc/sec.). This modulation appears at the crystal detector (Fig. 5.2a). If the center frequency of the klystron is shifted from that of the resonant cavity, the frequency of the voltage appearing at the crystal detector is 10 kc/sec. Its phase is dependent on whether the klystron center frequency is higher or lower than the resonant cavity frequency. The amplitude of this reflected 10 kc/sec signal depends on the relative difference between f_0 and f_r (see Fig. 5.2b and c). This error voltage is amplified by the a.c. amplifier (20), then phase detected (21). The result is a d.c. output voltage which is superimposed on the klystron reflector voltage as a correction voltage so that the center frequency of the klystron corresponds to the fre-

quency of the resonant cavity.

C. Detection:

In order to detect the EPR signal satisfactorily the magnetic field is modulated about the steady field position H_0 . The modulation signal is obtained from the reference voltage output of a Princeton Applied Research JB - 5 lock-in-amplifier, the frequency of which can be varied up to 100 kc/sec. The amplitude of this signal is variable and can be selected to suit any particular line.

The microwave energy, modulated at 200 c/sec which contains the EPR signal information, is detected by the IN 23 crystal detector in the detector arm. The resulting 200 c/sec signal is then fed into the PAR Lock-in-Amplifier and is detected in the manner described in the previous section. The PAR lock-in-amplifier is essentially a phase-sensitive amplifier which only amplifies signals having the same frequency and phase as the internal reference voltage. Thus much of the noise which accompanies the EPR signal is excluded. The d.c. output of the lock-in-amplifier, thus obtained, is the derivative of the actual absorption curve and is fed into the Chart-recorder.

D. Magnet:

The magnet used is a Newport seven inch electromagnet, type E. The gap between the pole pieces is adjustable and the poles carry universal screw shims. The

power supply for the magnet has been built in our laboratories, and is found to be stable enough for holding a dpph signal steady on the oscilloscope for any length of time. The magnetic field variation over the paramagnetic specimen is no more than 0.01% for the range of field that has been used in the present work.

The steady magnetic field is varied by fixing a small motor of suitable speed in conjunction with a set of gears to the helipot which changes the current in the magnet coils. The sweep rate is adjusted according to the nature of the spectrum. Although the variation of the magnetic field is not quite linear, this does not introduce any extra error as the position of each line has been measured individually for the final calculations. The steady magnetic field modulation is provided by coils wound in the same plane as that of the pole faces of the magnet. They are mounted side by side with the coils of the steady magnetic field, and are powered by a suitable frequency in the range of 200 c/s obtained from the commercial PAR lock-in-amplifier unit and a power amplifier.

E. Cavity and Goniometer:

The cavity which has been used in our spectrometer is made up of commercial x-band brass waveguide material, and is operated in the TE_{101} rectangular mode. The cavity is coupled to the waveguide through a coupling iris of 10^{-2} inch thick copper plate and has a coupling

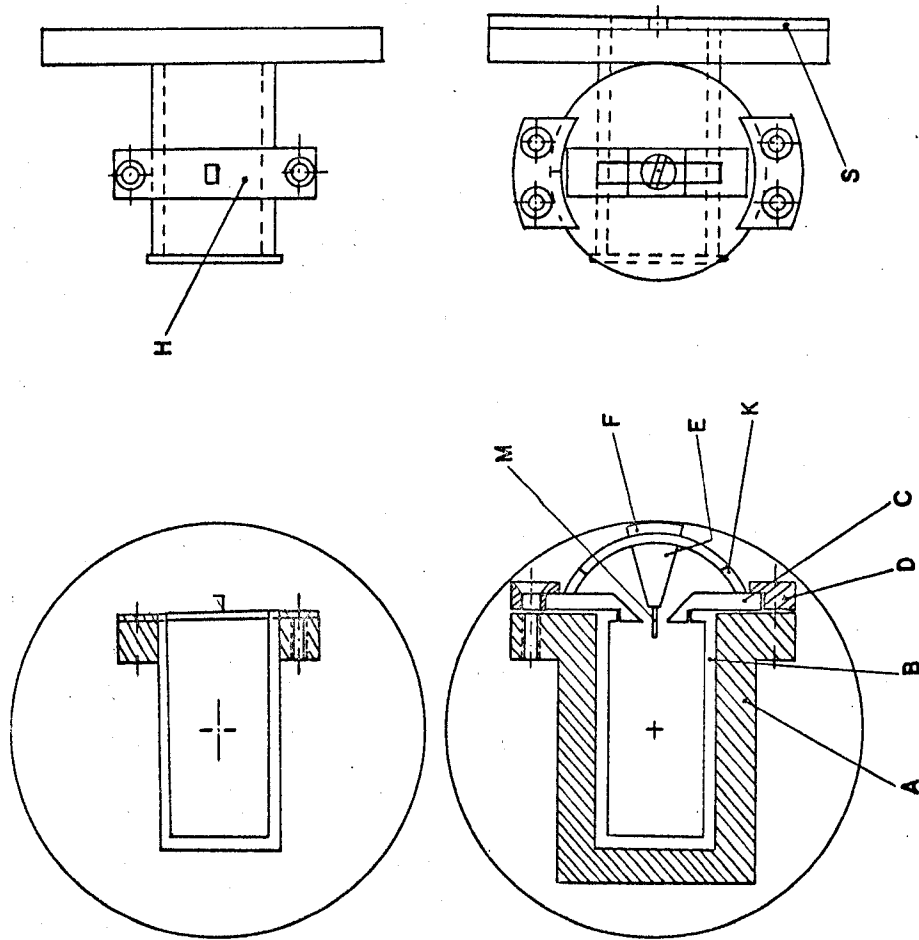


Fig. 5.3 Cavity Assembly

hole of approximately 0.15 inch in diameter. The cavity and the iris is gold plated to increase the Q of the cavity and to avoid deterioration by oxidation. A small coupling screw is attached to match the cavity. The Q of the cavity with the crystal mounted is found to be of the order of 1500 in our case. Fig 5.3 shows the cavity and its accessories.

The cavity is equipped with a goniometer which serves to orient the crystal with respect to the cavity walls. The goniometer C is fastened to the E-plane wall by means of a brass bracket composed of the parts A and D. The graduated plate C of the goniometer can be rotated through 360° about an axis normal to the E-plane of the cavity B. A semicircular track K is soldered to the graduated plate of the goniometer with its axis of rotation parallel to it. The track bears a brass runner which is composed of the parts E and F. A nylon pin M to which the crystal is glued is mounted on this brass runner.

CHAPTER VI

EXPERIMENTAL PROCEDURE

The experimental work consists of three different parts:

- A. Operation and adjustment of the spectrometer.
- B. Alignment of the crystal.
- C. Measurement of the magnetic field and klystron frequency.

A. Operation and Adjustment of the Spectrometer

To put the spectrometer into operation, the klystron is first tuned mechanically to give maximum output at the cavity resonant frequency. The signal klystron is modulated by a variable 60 c/sec signal on its reflector, and the reflected power from the cavity is viewed in an oscilloscope with the same 60 c/sec horizontal input, by means of a power take-off through a directional coupler. By adjusting the klystron cavity tuner and the reflector voltage, the frequency of the klystron is centered on the cavity resonance. This is indicated by an absorption dip in the klystron power mode at precisely the resonant frequency of the sample cavity. This frequency can be approximately measured by superimposing the wavemeter dip on the cavity absorption and noting the wavemeter reading. The wavemeter dip is then shifted from this

position to avoid any fluctuation. Once the klystron is tuned to the cavity frequency, the task remains to match the cavity impedance with that of the waveguide arm. A poor impedance match between the cavity and its arm of the hybrid-T causes a sharp reduction in the amount of power absorbed. The matching is effected by selecting a coupling iris of suitable size, and adjusting the coupling screw and the slide screw tuner.

It is to be noted that the cavity-matching depends on the sample, and as such for the final work the matching is done with the crystal properly adjusted in the desired orientation. After matching the cavity, the large 60 c/sec modulation is removed from the reflector, and is replaced by a very small 10 kc/sec modulation voltage. The klystron is now stabilized by varying the 4.5 volts continuous voltage on the reflector voltage supply battery bank until the frequency locks on. This is indicated by a minimum in the d.c. output of the IN 23 diode in the coupled arm.

The spectrometer is now ready for recording the spectrum. The magnetic field is now slowly varied and the spectrum is recorded on a x - y plotter whose input is driven by the output signal from a gaussmeter, Model REL 1890 whose Hall probe is placed very near to the cavity. The x-input is connected to the output of the PAR Lock-in-Amplifier. As the magnet is rotated about the waveguide axis, the pen is proportionately shifted

in the x-direction, thus enabling a complete angular variation of the spectrum to be recorded in one graph paper. The positions of the important resonance lines, necessary for exact calculations, are measured individually by locking the magnetic field at the center of the line concerned. The field is then measured by using NMR as explained in section (C).

B. Alignment of the Crystal

For the interpretation of the spectrum it is essential that the relation between the magnetic axes of the ion sites in the crystal and the magnetic field direction is completely known. Since the magnetic axes are usually related in a simple way to the crystallographic axes, it is easier to locate the crystallographic axes. The relations between the magnetic axes and crystallographic axes are then obtained from the angular variation of the spectrum.

Cordierite is an orthorhombic crystal and hence has three mutually perpendicular crystallographic axes. Its crystallographic axes were located by taking Laue photographs and using a Greniger chart in conjunction with a stereographic projection. The crystal was then transferred to the microwave goniometer without changing its orientation. Finally it was checked by mounting the microwave goniometer on the x-ray goniometer stand, and any necessary final adjustment was made by using the arc

of the microwave goniometer. The microwave goniometer was then fitted into the cavity and was locked in position by tightening the brass brackets. The lengths and positions of the waveguide components were so adjusted that the cavity lies just at the center of the magnet and the magnet can be freely rotated by 360° . The vertical arm containing the cavity was finally levelled by a spirit-level and a telescope to make it precisely vertical.

C. Measurement of Magnetic Field and Klystron Frequency

Methods of measuring the magnetic field have been comprehensively outlined by Symonds (1955), and the method chosen as the most suitable and readily usable is the proton magnetic resonance oscillator method. The sample is held in a seven millimeter diameter glass tube. The sample is water with a small amount of copper-sulphate in order to shorten the relaxation time of the resonance line. It is the proton of hydrogen in the water which is responsible for the resonance line. The probe proper consists of a calibrated marginal oscillator and a detector amplifier system. The modulation coils of the probe are supplied with the output of 60 c/sec sweep circuit whose maximum output is three volts peak to peak. Since the tunable frequency range of the oscillator with the commercial probe supplied was only from 8 to 22 mc/sec and we had to measure fields corresponding to the frequencies of 2.8 mc/sec up to about 7 mc/sec for the resonance lines

and about 12 mc/sec for the dpph line, we had to construct several probe heads with different numbers of turns in the r.f. coil for different ranges. For the lowest frequencies it was not possible to use water and a special probe was constructed using mineral oil as the source of protons.

To measure the magnetic field, the water sample is placed in the magnetic field very close to the cavity, the proton resonance signal is obtained by changing the frequency of the NMR oscillator and is displayed on an oscilloscope. The frequency of the marginal oscillator is measured by using a heterodyne frequency meter to obtain a zero beat pattern on the oscilloscope display. The frequency is then obtained from the calibration table. An accuracy of 1 in 10^5 is obtained for the oscillator frequency and also, therefore, for the magnetic field value.

The relationship between the proton resonance frequency and the value of the steady magnetic field is given by the equation

$$h\nu_p = \gamma H \quad (6.1)$$

Since γ and h are well known and since ν_p is the proton resonance frequency which is measured, the magnetic field can be obtained from the relation

$$H = h\nu_p / \gamma$$

or

$$H \text{ (k-gauss)} = \frac{1}{4.2577} \nu \text{ (mc/sec)} \quad (6.2)$$

The frequency of the klystron is obtained by observing the dpph signal. If the dpph signal occurs at field H , then the corresponding klystron frequency is given by

$$\nu = g\beta H/h \quad (6.3)$$

where β is the Bohr-magneton and g for dpph is 2.0036.

CHAPTER VII

RESULTS AND CALCULATION

A. Results

As has already been mentioned, only the spectrum due to Fe^{3+} , substitutionally occupying the position of Al in cordierite, has been analyzed in the present work. The angular variation of the Fe^{3+} spectra were recorded about all the three crystallographic axes at intervals of 15° .

Figs. 7.1 (a) and (b) represent the spectrum with the magnetic field perpendicular to the c-axis, along and 15° off the b-axis, respectively and show how the lines coalesce in pairs along the b-axis. Figs. 7.2(a) and (b) show the complete angular variation of the spectrum about the b and c crystallographic axes, respectively. At most orientations, the spectrum consists of three lines, two of which are more intense than the other. The more intense pair of lines varies little in intensity over the whole angular range. The minimum and maximum effective g-values for each are 3.2 and 5.1, respectively, and their angular variations are 60° out of phase. The weaker line varies rapidly in intensity and was only observable from the maximum g-value of 9.1 down to g approximately 4. Again, the angular variation consists of two curves 60° out of phase. The orientations at which the

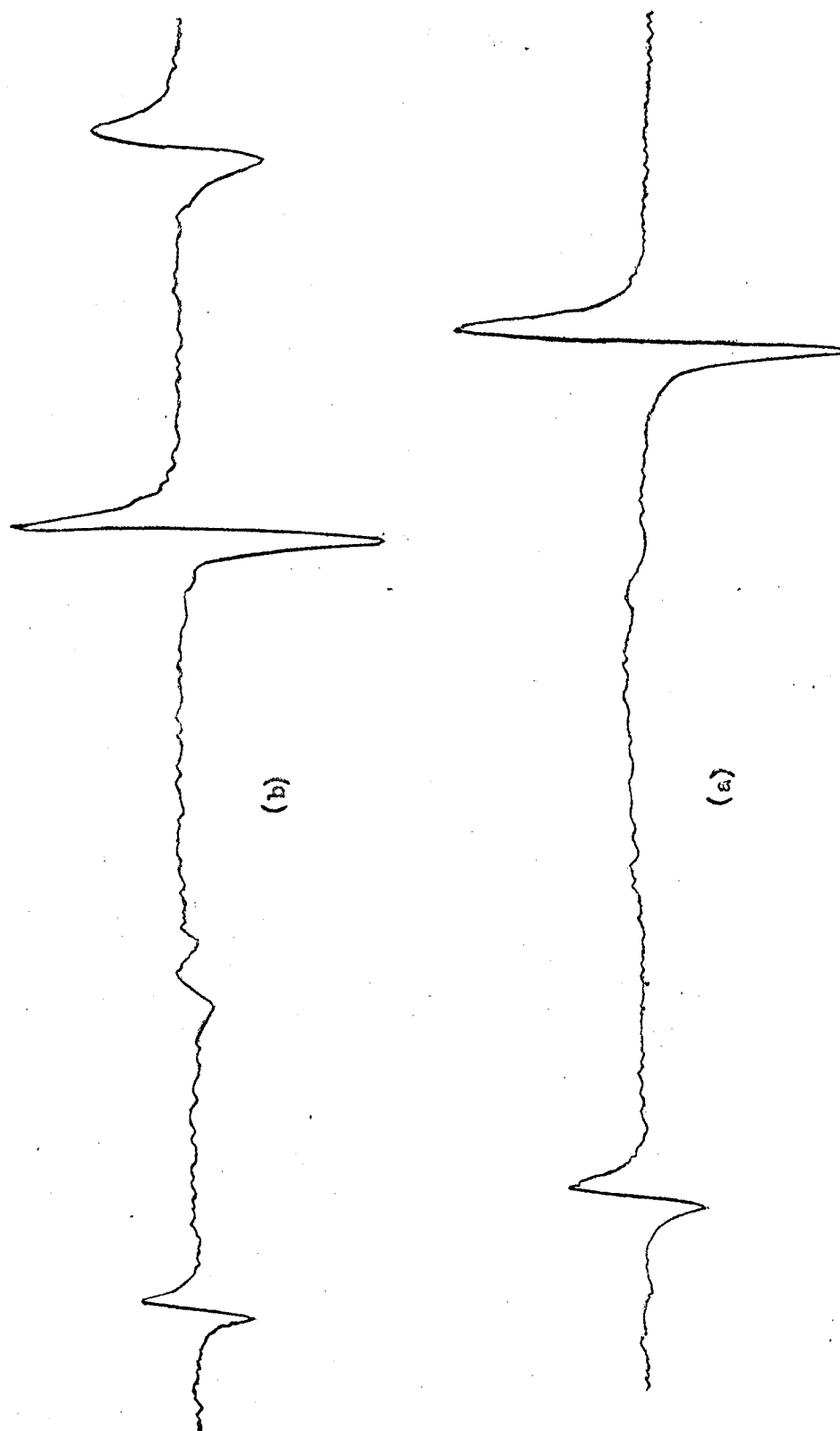


Fig. 7.1 Spectra of cordierite (a) along b axis (b) 15° away from b axis.

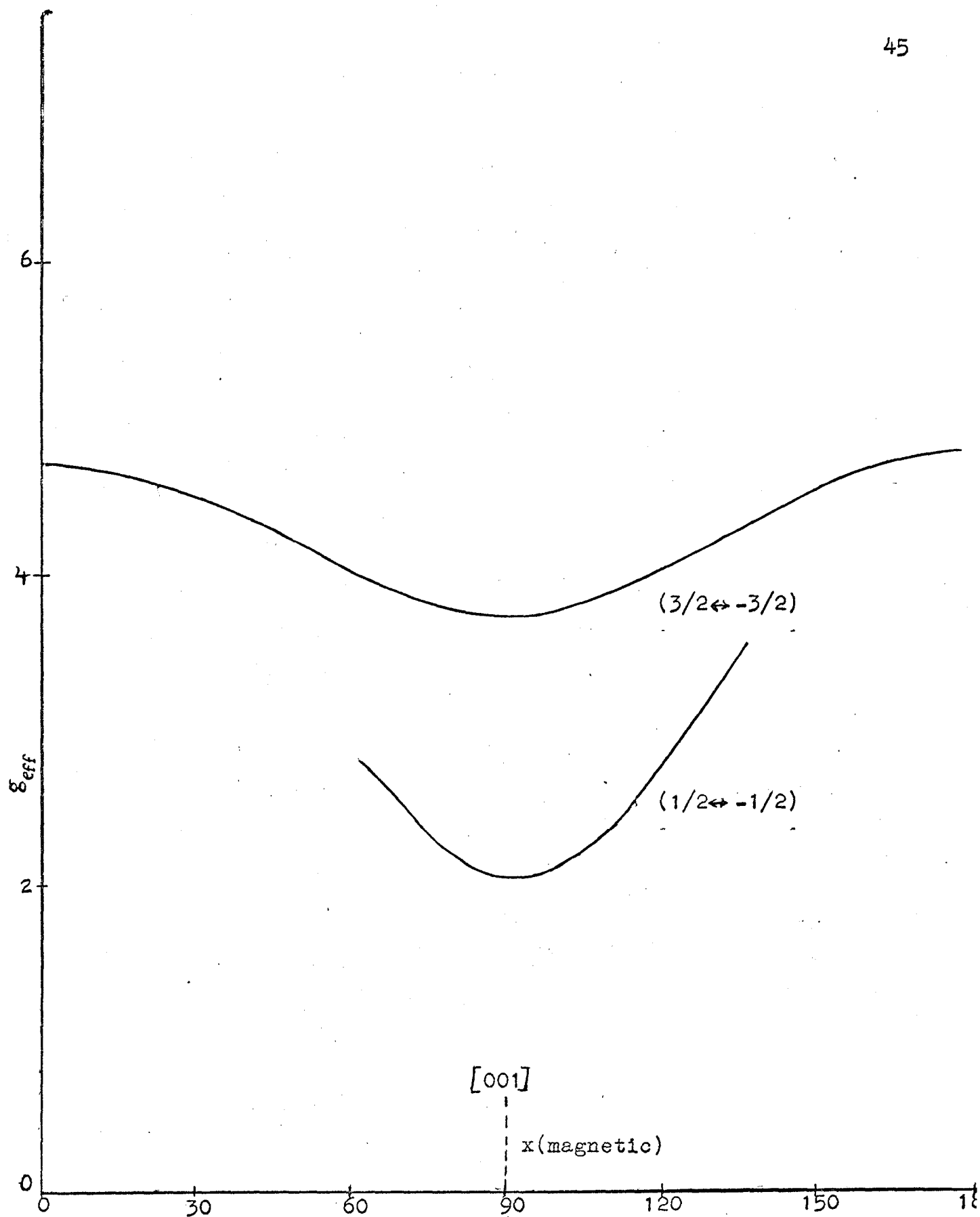


Fig 7.2a

Direction of the applied magnetic field (degrees).

Angular variation of g_{eff} values ($H \perp b$).

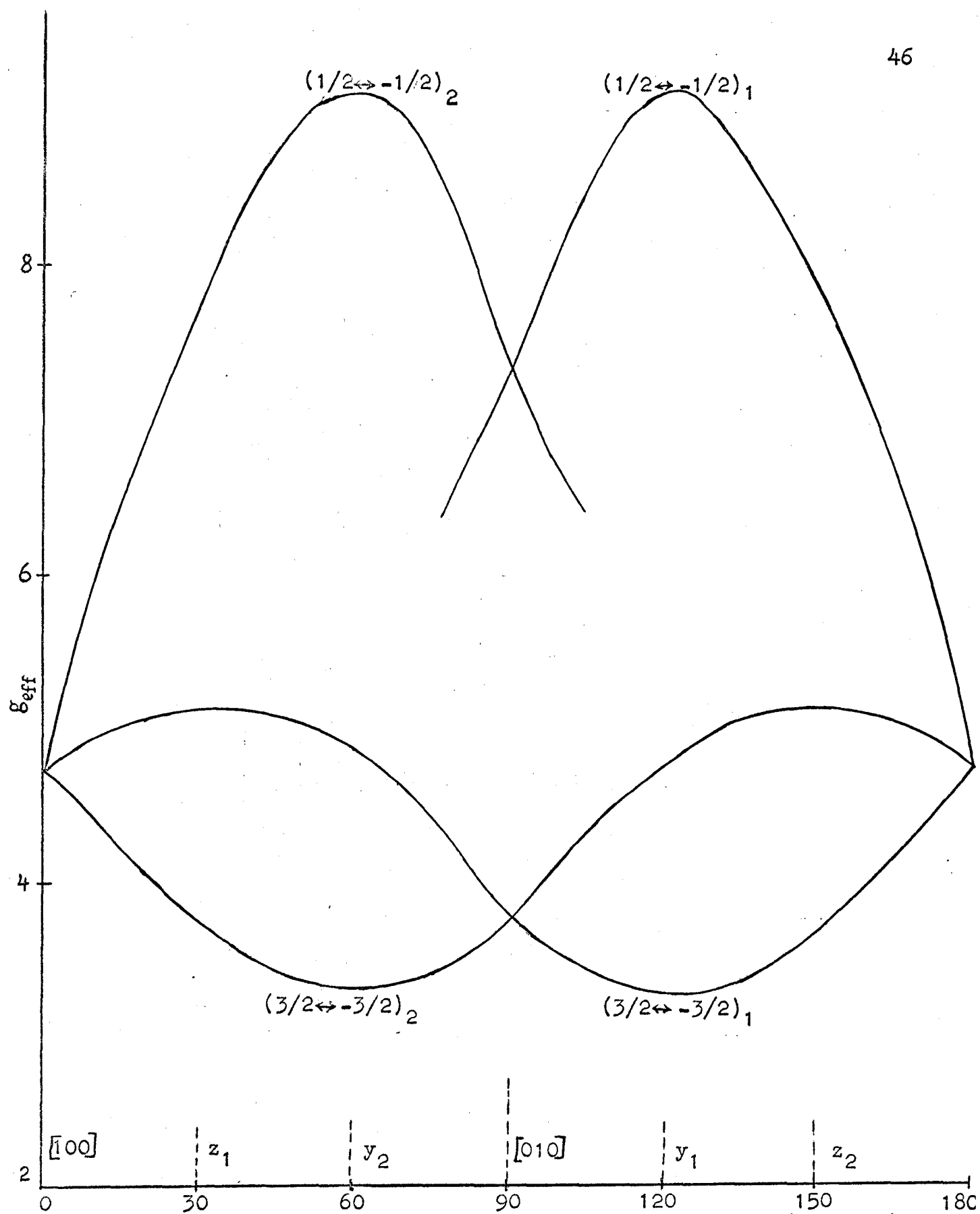


Fig 7.2b

Direction of the applied magnetic field (Degrees).

Angular variation of g_{eff} values ($H_{\perp} \text{ c}$).

weaker line has maximum g-value are the same as those for which the strong line has minimum g-value. The weak lines and the strong lines coincide when the magnetic field lies along the a-and-b-axes. From this behaviour, it may be concluded that the spectrum consists of two lines for each of two crystallographically equivalent sites, these sites being related on a 60° rotation about the c-axis.

The spectra about the a-and b-axes each contain only two lines, a strong line with comparatively little change in intensity or g-value, and a weak line observable over only a part of the rotation. In these cases, the spectra from the two sites are superimposed. This fact was verified by slightly misaligning the crystal in the a-rotation, when each line split into two.

As explained later, in each rotation, the strong and weak lines have been attributed to the $(\frac{3}{2} \leftrightarrow -\frac{3}{2})$ and $(\frac{1}{2} \leftrightarrow -\frac{1}{2})$ transitions, respectively, of Fe^{3+} occupying the (k) positions of aluminum. The magnetic axes for the two sites have been identified from the angular variation about the c-axis, and are indicated in Fig. 7.2(a) where the suffixes 1 and 2 refer to the two sites. The y and z magnetic axes make angles of 30° and 120° with respect to the b-axis, in opposite senses for the two sites. The x-axis is common to both sites and coincides with the c-axis.

The following are the experimentally measured resonant fields and effective g-values for the lines

along the x, y and z directions (Table 7.1).

TABLE 7.1
Position of the DPPH line - 3.1434 Kg

Direction	Transition	Site	Field (kg)	g_{eff}
y_1	$(\frac{3}{2} \leftrightarrow -\frac{3}{2})$	1	1.9498	3.228
	$(\frac{1}{2} \leftrightarrow -\frac{1}{2})$	1	0.6936	9.074
z_1	$(\frac{3}{2} \leftrightarrow -\frac{3}{2})$	1	1.2370	5.088
y_2	$(\frac{1}{2} \leftrightarrow -\frac{1}{2})$	2	0.6939	9.074
	$(\frac{3}{2} \leftrightarrow -\frac{3}{2})$	2	1.9449	3.236
z_2	$(\frac{3}{2} \leftrightarrow -\frac{3}{2})$	2	1.2392	5.079
x	$(\frac{3}{2} \leftrightarrow -\frac{3}{2})$	common	1.7069	3.683

B. Calculations

From the experimentally observed data it has been possible to determine the ratio of E/D and to make an estimate of D. All the calculations have been done by trial and error using an IBM 1620 computer.

An initial estimate for $\eta = \sqrt{3}$ E/D of 0.32 was made by referring to a set of calculations made by Dr. H. Ogata which employ second order perturbation theory

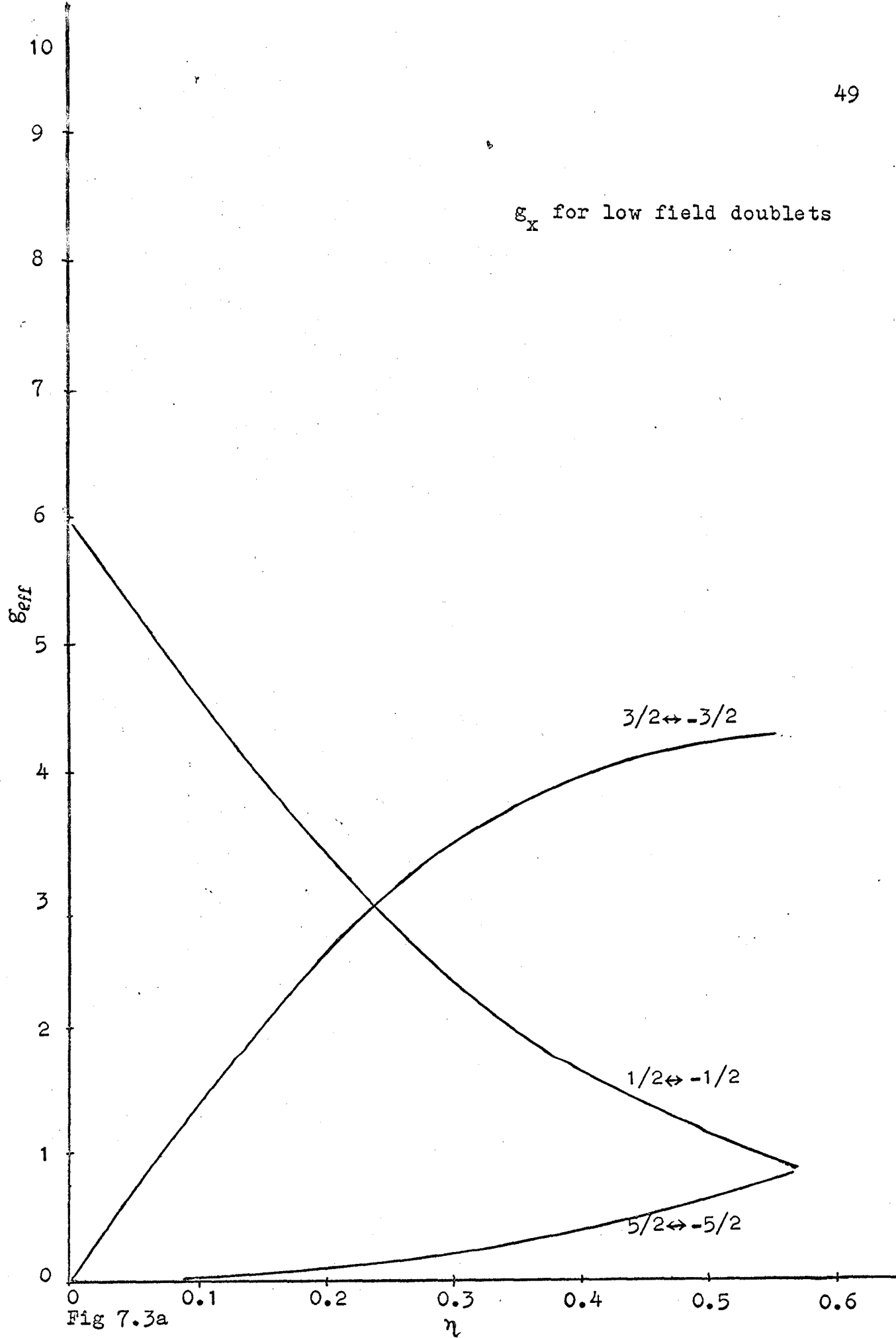


Fig 7.3a

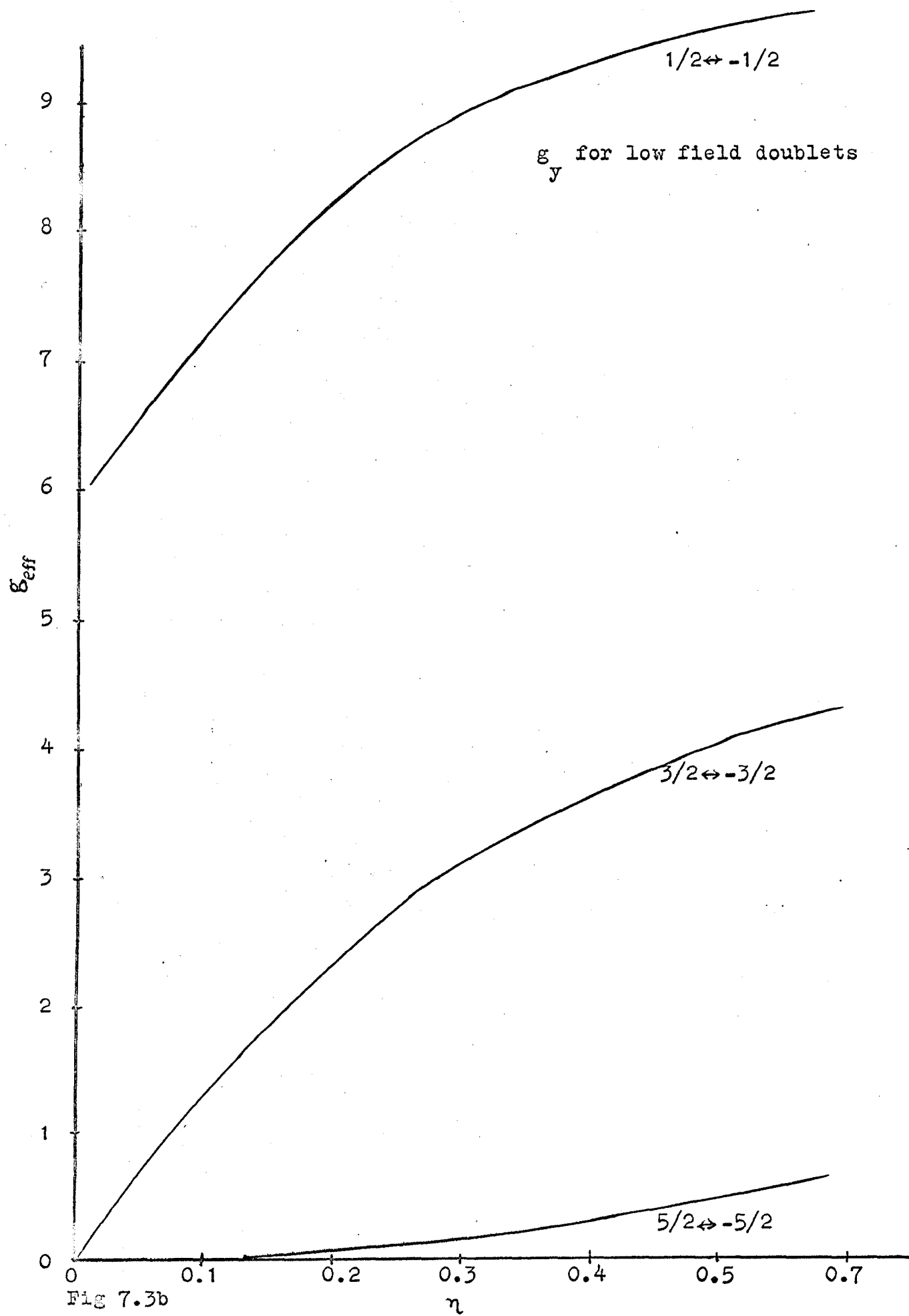


Fig 7.3b

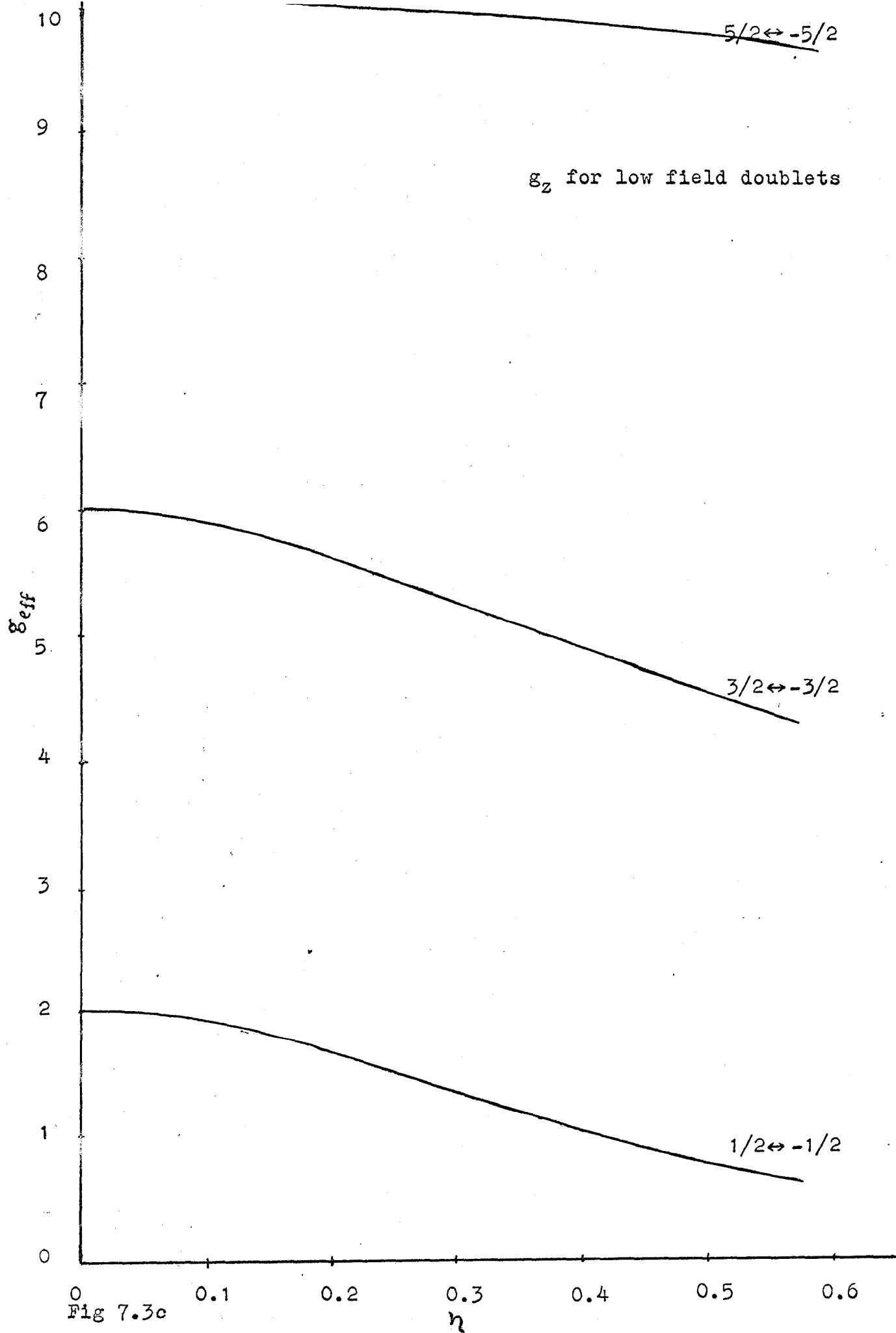


Fig 7.3c

to give g-values as a function of η for the low field doublets (Fig 7.3 a, b, c). These calculations are valid for the case where the effect of the magnetic field is small compared to that of the crystalline field. Comparison of the experimental g-values with these curves also enabled the magnetic axis to be assigned.

The final calculations were made by diagonalizing the Hamiltonian for each experimentally observed resonant field using different values of D and η . The energy level differences (in kg) were calculated and compared with the dpph resonant field. The values of D and η giving energy level differences closest to the dpph value for each case were recorded. This process was repeated for finer steps of D and η in a smaller range, and the results which best matched are shown in table 7.2. The values of D and η corresponding to the best match are taken.

TABLE 7.2

Direction	Field (kg)	H_{DPPH} (kg)	η	D (kg)
x	1.7069	3.1376	0.340	14.5
y	0.6936	3.1434	0.335	15.7
				18.7
	1.9474	3.1434	0.330	11.2
z	1.2381	3.1428	0.342	10.2
				10.5

From this η and D can be taken as

$$\eta = 0.335 \pm .005$$

$$E/D = 0.193 \pm 0.003$$

$$D = 15 \pm 5 \text{ kg}$$

C. Energy Level Diagram

To obtain the energy levels, the above values of η and D were substituted in the Hamiltonian matrix and the energy levels were calculated for magnetic fields from 0 kg to 20 kg and for all the three directions. In each case six energy values corresponding to the states $\pm \frac{5}{2}$, $\pm \frac{3}{2}$, $\pm \frac{1}{2}$ were obtained. The energy level diagrams for the three directions are shown in Fig. 7.4 a, b and c. From the energy level diagrams, the positions of the

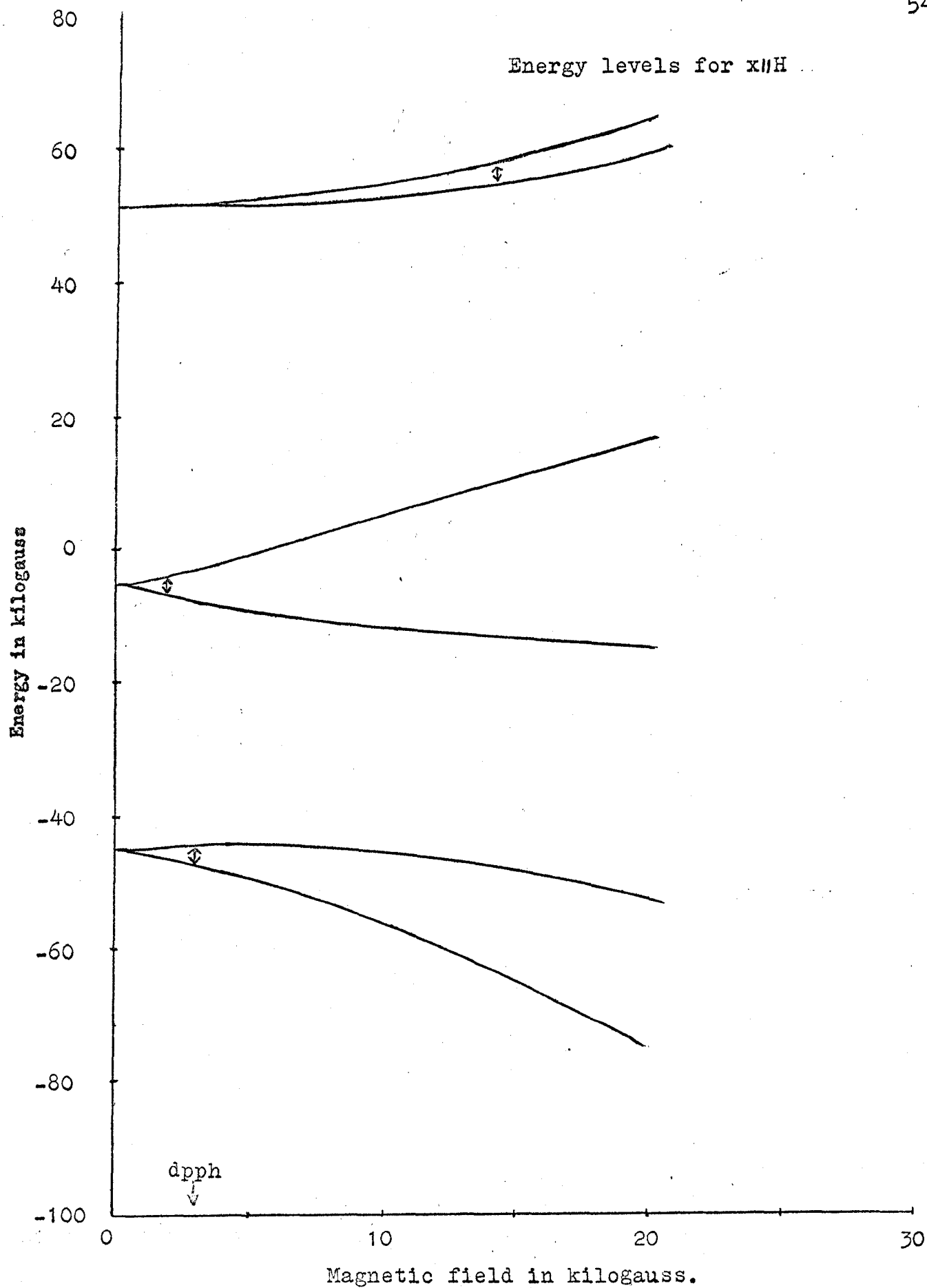


Fig 7.4a

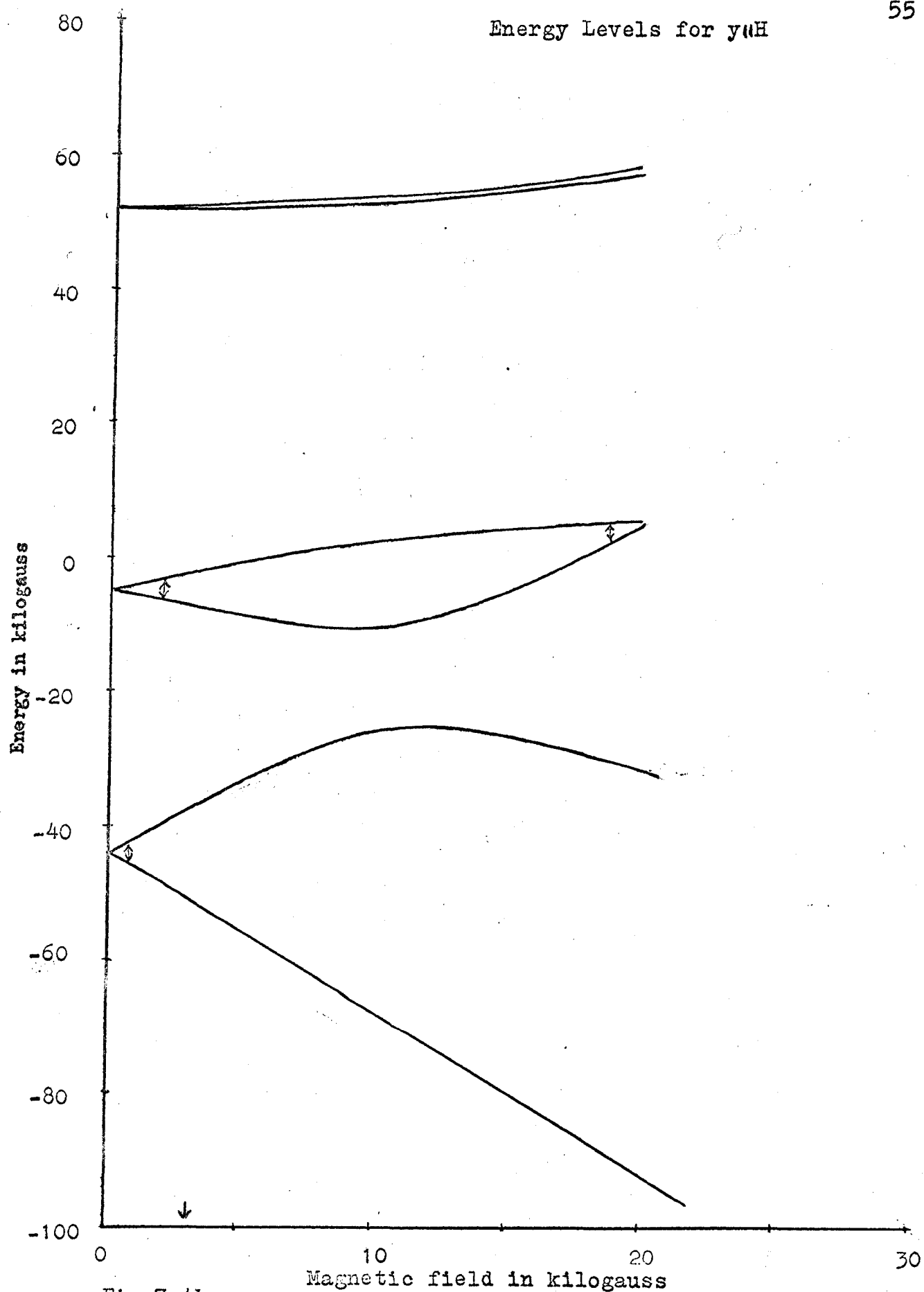
Energy Levels for γuH 

Fig 7.4b

Magnetic field in kilogauss

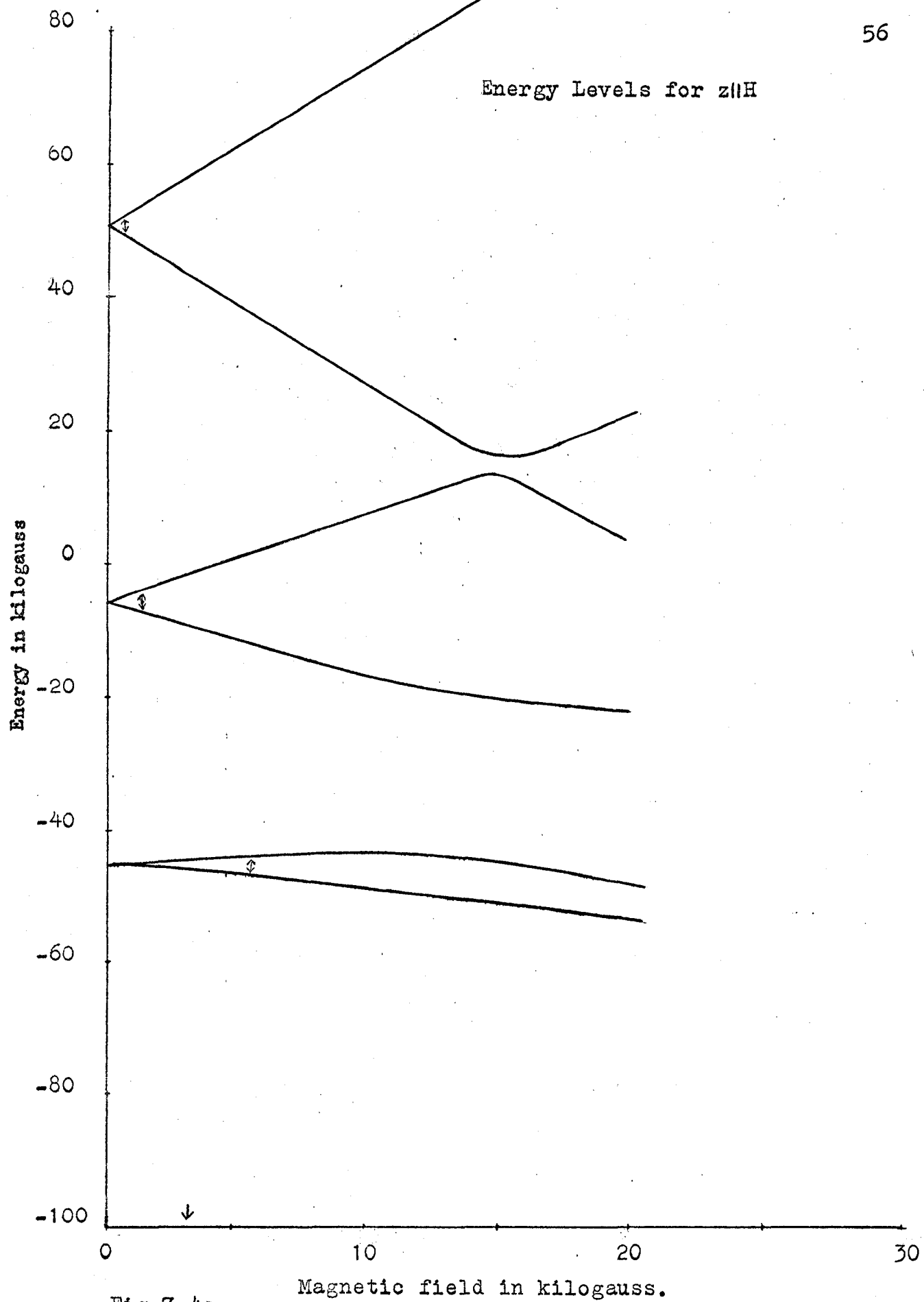


Fig 7.4c

observed transitions are obtained and are compared with the experimentally observed values which have excellent agreement in all directions. Table 7.3 shows the agreement between experimental values averaged over both the sites, and the predicted values.

TABLE 7.3

Direction	Transition	Av. Measured Value (kg)	Calculated Value (kg)
x	$(\frac{3}{2} \leftrightarrow -\frac{3}{2})$	1.7009	1.71
y	$(\frac{3}{2} \leftrightarrow -\frac{3}{2})$	1.9473	1.94
	$(\frac{1}{2} \leftrightarrow -\frac{1}{2})$	0.6937	0.69
z	$(\frac{3}{2} \leftrightarrow -\frac{3}{2})$	1.2381	1.24

C. Errors

There are two possible sources of errors in the present experiment: (i) alignment of the crystal (ii) setting of the field on the EPR line and determination of frequency by using heterodyne frequency meter.

(i) Alignment of the crystal. To avoid error due to misalignment, the crystallographic axes were rechecked after transferring the crystal to the microwave goniometer from the x-ray goniometer. Final setting was

done by observing the symmetry of the angular variation and the splitting of the lines. The last operation allowed us to set the crystal within $\pm 1^\circ$.

(ii) Setting of field and measurement of frequency.

The lines along the three principal axes were measured by adjusting the magnetic field to the centre of each line, indicated by the signal on the output meter of the lock-in-amplifier. The lines were located by approaching from both higher and lower fields in turn. The resonant field was then determined with n.m.r. The reproducibility of the n.m.r. frequency, as the field was changed and then reset on the line was within 4 kc/sec in an average frequency of 5 Mc/sec. In addition, the n.m.r. frequency was measured several times for each line; if possible using different harmonics with the heterodyne frequency meter. The overall reproducibility in these measurements was within 5 Kc/sec, corresponding to an uncertainty of ± 1 gauss in the field values.

CHAPTER VIII

CONCLUSIONS

From the foregoing discussion it is clear that the spectrum observed was due to Fe^{3+} occupying sites of Al in cordierite and experiencing a very high crystalline field. Although no chemical analysis were done to find out the impurity ion, the excellent agreement between the predicted and experimental data left little doubt about the nature of the impurity ion. From the crystal structure it would appear that there should be three different sets of spectra for Fe^{3+} corresponding to the three sets of aluminium in cordierite. In the actual experiment, however, only two sets of spectra are observed. This indicates that either the third site does not contain Fe^{3+} , or else the concentration is too small to give rise any observable intensity in the spectrum.

This may be due to the fact that the distance between the Al in the 4(b) position and the oxygen is 1.75\AA , whereas the distance between the Al in 8(k) and oxygen is 1.8\AA . Because of this smaller interatomic distance between the Al in 4(b) position and oxygen, the probability of Fe^{3+} replacing Al may be less than for the other two sites. In any case, the results indicate that the (b) and (k) sites are not equivalent. Thus the

observed spectra have been attributed to the Fe^{3+} ion located in the 8(K) positions, since their principal axes coincide with the 2-fold symmetry axes of Al in the (K) positions.

In the spectrum of cordierite no Zeeman transitions ($\Delta M = \pm 1$) has been observed. This is a consequence of the large value of D which separates the energy levels into three pairs, the energy gap between each pair being much greater than the separation within a pair. Consequently Zeeman transitions cannot be observed at the usual microwave frequencies in the X or K bands.

As regards the low field doublets, only $(\frac{3}{2} \leftrightarrow -\frac{3}{2})$ and $(\frac{1}{2} \leftrightarrow -\frac{1}{2})$ transitions have been observed. From the energy level diagram, the $(\frac{5}{2} \leftrightarrow -\frac{5}{2})$ transition is expected either at very low or at very high fields. However, no such transition has been observed. The transition probabilities are expected to vary considerably with orientation (Holuj - 1965), but no calculations of them have been carried out.

Since only limited number of experimental data were available, it was not possible to obtain all the parameters in the spin Hamiltonian. The only quantities that have been obtained are

$$E/D = 0.193 \pm 0.003$$

$$D = 15 \pm 5 \text{ kg}$$

It is expected that the experiments in K-band

will reduce the uncertainty in the D value significantly. The future plan includes the work in K-band and also analysis of the Mn^{2+} spectrum, which has already been observed. Work at low temperatures should enable the sign of D to be determined. This may also show the spectrum due to Fe^{2+} which is expected to be present substitutionally in place of magnesium.

BIBLIOGRAPHY

- Abraham, A., and Pryce, M. H. L. 1951. Proc. Roy. Soc. A205, 135.
- Al'tshuler, A. A., and Kozyrev, B. M. 1964. Electron Paramagnetic Resonance. Acad. Press.
- Bagguley, D. M. S., and Owen, J. 1957. Rep. Prog. Phy. 20, 304.
- Bagguley, D. M. S., and Griffith, J. H. E. 1947. Nature. 160, 532.
- Barry, T. I., McNamara, P., and Moore, W. J. 1965. J. Chem. Phy. 42, 2599.
- Bennet, J. E., Gribson, J. F., and Ingram, D. J. E. 1957. Proc. Roy. Soc. A240, 67.
- Bleaney, B., and Bowers, K. D. 1952. Proc. Roy. Soc. A214, 451
- Bleaney, B., and Stevens, K. W. H. 1953. Rep. Prog. Phy. 16, 107.
- Bowers, K. D., and Owen, J. 1955. Rep. Prog. Phy. 18, 305.
- Bystrom, A. 1941. Ark. Kemi. Min. Geol. 15B, 7.
- Castner, T., Newell, G. S., and Holton, W. C. 1960. J. Chem. Phy. 32, 668.
- Cummerow, R. L., and Halliday, D. 1946. Phy. Rev. 70, 433.
- Dana, J. Manual of Mineralogy. 1959. John Wiley & Sons
- Feher, G. 1957. B. S. T. J. 36, 450.
- Geusic, J. E., Martin, P., and Schulz-Du Bois, E. O. 1959. B. S. T. J. Jan., 291.
- Griffith, J. S. 1959. Proc. Roy. Soc. A235, 23.
- Holuj, F. 1965. Can. J. Phy. 43, 727.
- Low, W. 1960. Paramagnetic Resonance in Solids. "Solid State Phy. Suppl. 2."

- Pake, G. E. 1960. Paramagnetic Resonance. Benjamin Pub.
- Pryce, M. H. L. 1950. Proc. Phy. Soc. A63, 25.
- Pryce, M. H. L. 1950. Phy. Rev. 80, 1107.
- Sands, R. H. 1955. Phy. Rev. 99, 1222.
- The Varian Associates - NMR - EPR Staff. 1960. NMR and EPR Spectroscopy. The Macmillan Company.
- Wickman, H. H., Klein, M. P., and Shirley, D. A. 1965. J. Chem. Phys. 42, 2113.
- Zavoyskiy, E., 1945. J. Phys. USSR. 9, 211.

VITA AUCTORIS

- 1938 Born in Dumka, Bihar, India.
- 1955 Completed high school education from Dumka Zila School, Dumka, Bihar, India.
- 1961 Received the Degree of Master of Science in Physics from Ranchi University, Ranchi, India.
- 1965 Currently a candidate for the Degree of Master of Science in Physics at the University of Windsor, Windsor, Ontario, Canada.